

See discussions, stats, and author profiles for this publication at: <https://www.researchgate.net/publication/236183272>

Kinetics and Mechanism of the Tropospheric Oxidation of Vinyl Acetate Initiated by OH Radical: A Theoretical Study

ARTICLE *in* THE JOURNAL OF PHYSICAL CHEMISTRY A · APRIL 2013

Impact Factor: 2.69 · DOI: 10.1021/jp3126736 · Source: PubMed

CITATIONS

13

READS

17

4 AUTHORS, INCLUDING:



[Debasish Mandal](#)

Hebrew University of Jerusalem

29 PUBLICATIONS 153 CITATIONS

[SEE PROFILE](#)



[Chandan Sahu](#)

11 PUBLICATIONS 34 CITATIONS

[SEE PROFILE](#)

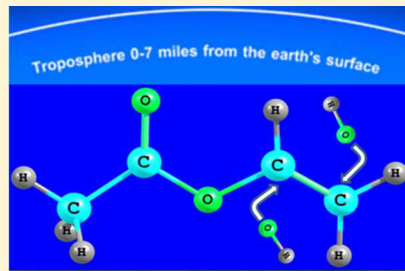
Kinetics and Mechanism of the Tropospheric Oxidation of Vinyl Acetate Initiated by OH Radical: A Theoretical Study

Debasish Mandal, Chandan Sahu, Sabyasachi Bagchi, and Abhijit K. Das*

Department of Spectroscopy, Indian Association for the Cultivation of Science, Jadavpur, Kolkata 700 032, India

S Supporting Information

ABSTRACT: Vinyl acetate [VA ($\text{CH}_3\text{COOC}_2\text{H}_3$)] is an important unsaturated and oxygenated volatile organic compound responsible for atmospheric pollution. In this work, possible reaction mechanisms for the degradation of OH-initiated atmospheric oxidation of VA are investigated. The potential energy surfaces (PESs) for the reaction of OH radical with VA in the presence of O_2 and NO have been studied using the M06-2X/6-311++G(d,p) method. The initial addition reactions of more and less substituted ethylenic C-atoms of VA are treated separately, followed by a conventional transition state theory (TST) calculation for reaction rates. The direct H-abstraction mechanism and kinetics have also been studied. The initial OH addition occurs through a prereactive complex, and the calculated rate constants in the temperature range 250–350 K for both the addition reactions are found to have negative temperature dependence. The calculation indicates that the reaction proceeds predominantly via the addition of OH radical to the double bond rather than the direct abstraction of H-atoms in VA. IM1 [$\text{CH}_3\text{C}(\text{O})\text{O}^*\text{CH}_2\text{OH}$] and IM2 [$\text{CH}_3\text{C}(\text{O})\text{OCH(OH)}^*\text{CH}_2$], the OH adduct complexes formed initially, react with ubiquitous O_2 followed by NO before their rearrangement. The formation of the prereactive complex plays an important role in reaction mechanism and kinetics. The calculated rate constant, $k_{298\text{K}} = 1.61 \times 10^{-11} \text{ cm}^3 \text{ molecule}^{-1} \text{ s}^{-1}$, is well harmonized with the previous experimental data, $k_{298\text{K}} = (2.48 \pm 0.61) \times 10^{-11} \text{ cm}^3 \text{ molecule}^{-1} \text{ s}^{-1}$ (Blanco et al.) and $k_{298\text{K}} = (2.3 \pm 0.3) \times 10^{-11} \text{ cm}^3 \text{ molecule}^{-1} \text{ s}^{-1}$ (Picquet-Varrault et al.). Additionally, consistent and reliable enthalpies of formation at 298.15 K ($\Delta_f H^\circ_{298.15}$) have been computed for all the species involved in the title reaction using the composite CBS–QB3 method. The theoretical results confirm that the major products are formic acetic anhydride, acetic acid, and formaldehyde in the OH-initiated oxidation of VA in the presence of O_2 and NO, which are in excellent agreement with the experimental findings.



INTRODUCTION

Vinyl acetate (VA) is one of the important unsaturated and oxygenated volatile organic compounds (OVOCs) released into the troposphere by anthropogenic and biogenic sources and is a significant atmospheric pollutant.^{1,2} Vinyl acetate is also considered as one of the high (H) production (P) volume (V) chemicals listed in the OECD (Organization for Economic Co-Operation and Development) integrated database.³ It may also be produced in the troposphere by the oxidation of alkanes, alkenes, etc.^{4–6} VA is extensively used in industry because its monomer is mainly required for the production of polyvinyl acetate and vinyl acetate copolymers that are used in water based paints, adhesives, etc.^{7,8}

The release of VA possibly takes place during commercial production and storage of VA or during preparation of different derivative polymers. Because of its numerous applications and high volatility, it can contribute to air pollution and also to photochemical smog events. Thus, a better understanding is required to determine the atmospheric reactivity of VA. From previous literature, it was found that VA possesses high vapor pressure, and consequently it exists as vapor when emitted into the atmosphere.³ Also, VA does not absorb sunlight in the atmospheric actinic region after being released into the troposphere and is expected to be oxidized by the OH radical in the presence of O_2 and NO.⁹

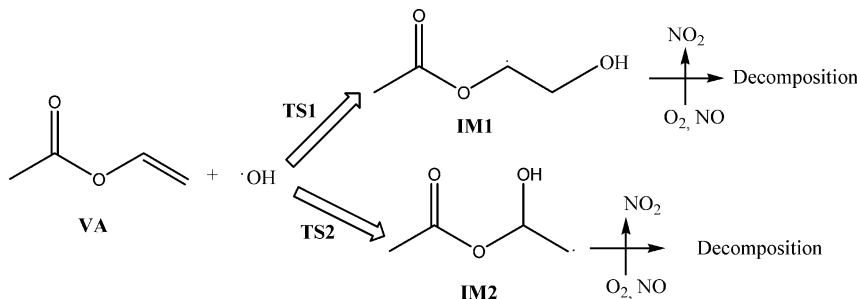
Unsaturated OVOCs are very reactive because of the presence of the double bond that is extremely receptive to the tropospheric oxidants, OH, NO_3 , and O_3 , which initiate their degradation. The experimental rate constants (measured at atmospheric pressure) suggest that photochemically produced OH radical is the most dominant oxidizing agent for VA in the troposphere.¹⁰ Therefore, information on the rate coefficients and the mechanism for the OH-initiated oxidation of VA in the presence of O_2 and NO will assist in determining their effects on atmosphere. Blanco et al.¹¹ experimentally investigated the OH-initiated degradation kinetics of VA and measured the rate constant as a function of temperature in the range 287–313 K. They also reported that rate coefficients possess a negative temperature dependence and low pre-exponential factor. Recently, Picquet-Varrault et al.¹⁰ published an experimental kinetics study of the OH-initiated oxidation of VA and identified and quantified the major products using the infrared spectroscopic technique.

The atmospheric oxidation of VA leads to the formation of formaldehyde (HCHO), formic acetic anhydride [FAA ($\text{CH}_3\text{CO}(\text{O})\text{CHO}$)], and acetic acid (CH_3COOH) as the

Received: May 18, 2012

Revised: April 5, 2013

Published: April 15, 2013

Scheme 1. Probable Reaction Pathways for OH-Initiated Oxidation of VA in Presence of O₂ and NO**Table 1.** Zero Point Energies (ZPE, in hartree), T1 Diagnostic Values, Total Energies (in hartree), and Relative Energies (in hartree) of Various Species in the OH-Initiated Oxidation of Vinyl Acetate in Presence of O₂ and NO

species	ZPE	E(M062X/BS1)	T1 dig.	$\langle S^2 \rangle$		E(CBS-QB3)	ΔE [M062X/BS1]
				before annihilation	after annihilation		
OH + VA	0.103659	-382.157175	0.01,0.01	0.75 0.0	0.75,0.0	-381.643942	0
O ₂	0.004040	-150.308614	0.015	2.0120	2.001	-150.163822	
NO	0.004764	-129.880285	0.025	0.7539	0.7500	-129.747452	
NO ₂	0.009239	-205.050715	0.026	0.7550	0.7500	-204.851479	
HO ₂	0.014639	-150.890590	0.030	0.7547	0.7500	-150.740241	
H ₂ O	0.021628	-76.420888	0.010	0.000	0.000	-76.337184	
HCHO	0.027147	-114.487213	0.017	0.0000	0.000	-114.343489	
CH ₃ CO ₂ H	0.062655	-229.064862	0.016	0.0000	0.000	-228.764331	
FAA	0.071362	-342.371233	0.017	0.0000	0.000	-341.938401	
R	0.106368	-382.167763	0.024	0.7533	0.7500	-381.649767	-0.007879
TS1	0.106285	-382.162366	0.028	0.7703	0.7501	-381.648241	-0.002565
TS2	0.106069	-382.161616	0.029	0.7679	0.7501	-381.648514	-0.002031
TSC1-P	0.101482	-382.049119	0.020	0.7592	0.7500	-381.639779	0.108056
TSC1	0.101463	-382.15039	0.020	0.7595	0.7500	-381.707079	0.004587
TSC4	0.100257	-382.14592	0.026	0.7620	0.7501	-381.636999	0.007851
TSC3	0.100892	-382.14368	0.026	0.7595	0.7501	-381.692858	0.01072
IM1	0.110548	-382.211599	0.017	0.7548	0.7500	-381.689096	-0.047535
IM2	0.109748	-382.220893	0.015	0.7550	0.7500	-381.699895	-0.057629
P1	0.081716	-305.76637	0.020	0.7595	0.7501	-305.339314	76.368861
P2	0.081221	-305.74153	0.028	0.7666	0.7501	-305.314760	76.393205
P3	0.081599	-305.74416	0.029	0.7635	0.7501	-305.317162	76.390953
IM3	0.121069	-532.579451	0.022	0.7550	0.7500	-531.909071	-150.40486
IM4	0.129984	-662.494358	0.020	0.0000	0.0000	-661.695836	-280.31085
IM4-T	0.129955	-662.497658	0.019	0.0000	0.0000	-661.697761	-280.31418
IM5	0.115396	-457.430181	0.020	0.7548	0.7500	-456.831730	-75.261269
IM6	0.048995	-228.367002	0.020	0.7534	0.7500	-228.076080	153.735509
IM7	0.058867	-378.731245	0.024	0.7544	0.7500	-378.291290	3.381138
IM8	0.068047	-508.660040	0.022	0.0000	0.0000	-508.091746	-126.53847
IM9	0.053719	-303.583871	0.073	0.7544	0.7500	-303.218541	78.523364
IM10	0.037587	-115.042930	0.017	0.7547	0.7500	-114.887807	267.048173
IM11	0.049718	-265.412119	0.026	0.7549	0.7500	-265.105886	116.691115
IM12	0.121388	-532.587976	0.022	0.7550	0.7500	-531.917110	-150.41307
IM13	0.130045	-662.503445	0.020	0.0000	0.0000	-661.704258	-280.31988
IM14	0.115434	-457.433697	0.017	0.7540	0.7500	-456.834631	-75.264747
IM15	0.081190	-342.911789	0.018	0.7544	0.7500	-342.467725	39.222917
IM16	0.092407	-493.284203	0.023	0.7547	0.7500	-492.692309	-111.13828
TS3	0.128845	-662.474624	0.017	0.0000	0.0000	-661.677447	-280.29226
TS4	0.113112	-457.419064	0.022	0.7632	0.7501	-456.825417	-75.252436
TS5	0.110905	-457.403791	0.026	0.7574	0.7500	-456.816858	-75.23937
TS6	0.044152	-265.383444	0.028	0.7568	0.7500	-265.086085	116.714224
TS7	0.113293	-457.411450	0.025	0.7666	0.7501	-456.817698	-75.244641
TS8	0.087210	-493.265325	0.027	0.7569	0.7500	-492.680871	-111.12459

major products. A number of experimental studies are found in the literature for the atmospheric chemistry of VOCs toward

different tropospheric oxidants.^{12–18} To the best of our knowledge, no theoretical study is found in the literature for

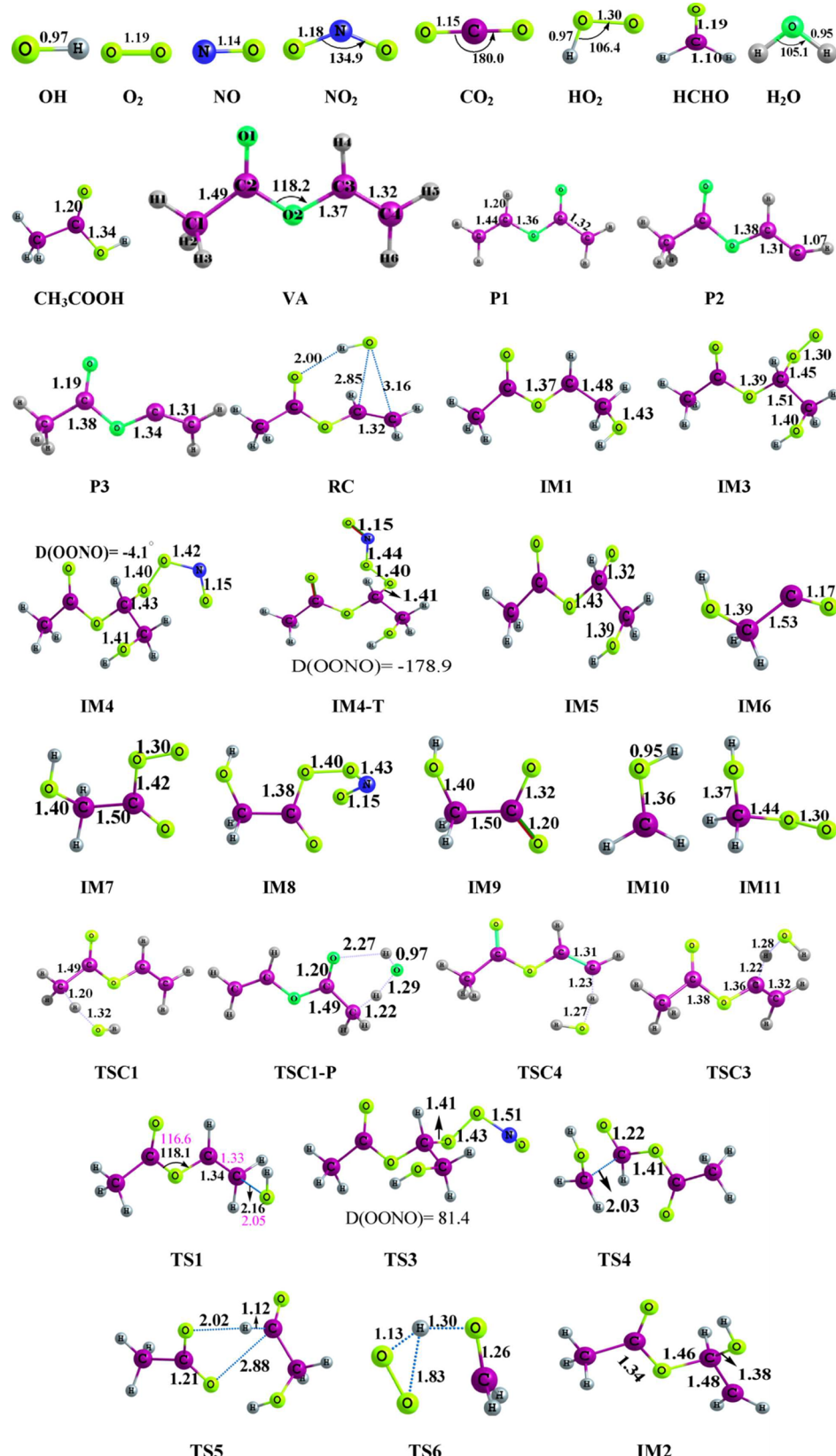


Figure 1. Optimized geometries with geometrical parameters calculated at M06-2X/BS1 level for the species involved in the terminal OH-initiated oxidation of vinyl acetate in presence of O₂ and NO addition reaction.

the mechanism and kinetics of vinyl acetate or any ester. However, there are a large number of theoretical investigations

for the atmospheric oxidation of OVOCs and other related compounds.^{19–27}

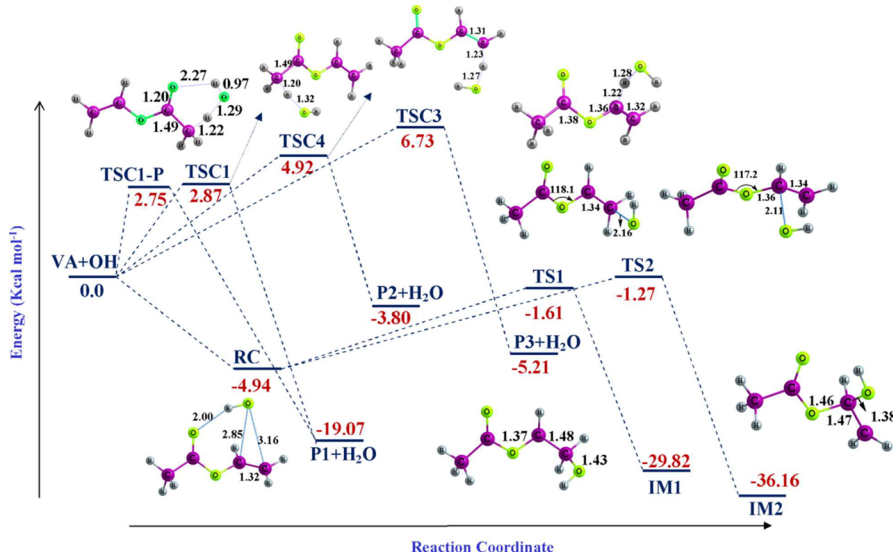


Figure 2. M062X/BS1 calculated potential energy (ZPVE corrected) profile for the terminal and internal addition of OH to VA.

To verify the experimental observations and to get more insights into the oxidation process, we have carried out a theoretical study on the OH-initiated oxidation of VA. In this work, density functional and ab initio molecular orbital calculations are performed to provide a detailed theoretical understanding of the mechanism and kinetics of the aforementioned oxidation process.

VA contains two unsaturated carbon atoms and various C-H bonds. Consequently, two types of initial reaction mechanism, e.g., hydrogen abstraction by OH radical and addition of OH to the double bond, will be investigated. It is found in our investigation that the OH addition reaction is more prominent than the H-abstraction route. However, the H-abstraction pathways have also been studied here in detail. The atmospheric chemical transformation process of VA may be thought of as depicted in Scheme 1. In the initial step of the oxidation, the OH radical may be added to the terminal or internal carbon of the double bond and produces two radicals, IM1[$\text{CH}_3\text{C}(\text{O})\text{O}^*\text{CHCH}_2\text{OH}$] and IM2[$\text{CH}_3\text{C}(\text{O})\text{OCH}^*(\text{OH})\text{CH}_2$]. Finally, various products are formed during reaction or rearrangement of IM1 and IM2 in the presence of O_2 and NO.

The main objective of the present study is to investigate the complete reaction mechanism, focusing on the key reaction steps such as OH addition to VA, O₂ addition to VA-OH, further rearrangement and elimination, etc. and to correlate our results with the recent experimental findings.^{10,11} The kinetics of the initial OH addition and H abstraction reactions are performed. We have studied the global PES of the reaction using a high level density functional M06-2X/6-311+G(d,p) method. The thermochemical studies have been performed to analyze the stability of all the species involved in the reaction. To have a clear picture of the total reaction mechanism, we have treated the whole reaction step by step.

COMPUTATIONAL DETAILS

The geometries of all molecular species involved in this study are fully optimized by employing density functional M06-2X²⁸ method in conjunction with the Pople's split-valence triple- ζ quality 6-311++G(d,p)²⁹ basis set (BS1) for all the elements. Zhao and Truhlar²⁸ recently developed the M06 family of local

(M06-L) and hybrid (M06, M06-2X) meta-GGA functionals that show promising performance for the kinetic and thermodynamic calculations without the need of refining the energies by post Hartree–Fock methods, and these functionals have been applied successfully in the recent studies.^{30,31} The M06-2X is a hybrid meta-DFT method with a high percentage of HF exchange, and it has broadest applicability with average mean absolute errors of about 1.3, 1.2, and 0.5 kcal/mol for thermochemical, barrier height, and noncovalent interaction calculations,³² respectively. The 6-311++G(d,p) is a valence triple- ζ quality basis set with single polarization and double diffuse functions on all atoms.

Harmonic vibrational frequencies are determined at the same levels of theories to confirm whether the optimized structures are local minima (no imaginary frequency) or transition states (one imaginary frequency) on the potential energy surfaces (PESs) and to evaluate the zero point vibrational energy (ZPVE) and thermal corrections to the Gibbs free energy at $T = 298$ K. The connecting first order saddle points, the transition states between the equilibrium geometries, are obtained by the synchronous transit-guided quasi-Newton (STQN) method. Parallel intrinsic reaction coordinate (IRC)^{33,34} calculations are performed with all transition states to confirm whether these transition states connect the right minima or not.

Additionally, the T1 diagnostic^{35,36} calculations are performed to verify the reliability of the results of the single-reference QCISD(T) wave function. It is known that the species having T1 values above 0.044³⁶ are considered to be somewhat less reliable. Examining the T1 values in Table 1, we see that all species have T1 values below the 0.030 value of HO₂ except three species. Fortunately, the energetics of these three species are not important in the present study. So the single-reference QCISD(T) wave function is expected to yield reliable energetics.

We also calculated the expectation values of the S^2 operator, $\langle S^2 \rangle$, to check the spin contamination for all the species because unrestricted electronic structure wave functions are not the eigenfunctions of the S^2 operator and may give $\langle S^2 \rangle$ values that deviate much from the true $\langle S^2 \rangle = 0.75$ for doublet species. The severe spin contamination could lead to a worse estimate of the barrier height.^{37,38} We examine spin contamination before and

after annihilation for all the species involved in the title reaction and see that for most of the species the $\langle S^2 \rangle$ values after annihilation range from 0.75 to 0.76.

The enthalpies of formation for all the species involved in the title reaction at 298.15 K ($\Delta_f H^\circ_{298.15}$) are calculated using CBS–QB3³⁹ electronic energies. The complete basis set CBS–QB3 method normally uses optimized geometry and frequencies calculated at the B3LYP/6-311G(2d,p) level, and then the MP2/6-311+G(2df,2p) energy and CBS extrapolation are computed. Because of the problem of convergence, which may arise because of the large self-interaction error in B3LYP calculation, for some TSs, the CBS–QB3 multilevel calculation has been improved for these systems where the optimized geometry and frequencies obtained by the B3LYP/6-311G(2d,p) method are replaced by those obtained by the M06-2X/6-311++G(d,p) method. The reliability of this method is verified by comparing the calculated enthalpies with the experimentally observed values. This kind of modification has worked successfully in a recent investigation.⁴⁰ The atomization scheme⁴¹ has been employed for the calculation of $\Delta_f H^\circ_{298.15}$, and for this purpose we have used the literature values⁴² of $\Delta_f H^\circ_{298.15}$ for C [171.29 kcal/mol], H [52.10 kcal/mol], O [59.51 kcal/mol], and N [113.08 kcal/mol].

The kinetics for the addition of OH to the ethylenic carbon of VA is evaluated using the well-known conventional transition state theory (TST). The details are given in the respective section.

All electronic structure calculations are performed using the Gaussian 09 suite of quantum chemistry programs.⁴³

■ RESULT AND DISCUSSION

The reaction of OH with VA can proceed through two possible pathways: the direct hydrogen abstraction and addition of OH radical to the double bond. These two pathways will be investigated here step by step.

H-Atom Abstraction Pathways. The M062X/BS1 optimized geometries and the PES are shown in Figure 1 and Figure 2, respectively.

The energies calculated at the M062X/BS1 level of theory for all the species, ZPE at the same level, S^2 values before and after annihilation, CBS–QB3 energies, relative energies (ZPE corrected) estimated at the M062X/BS1 level of theory, and the T1 diagnostic values calculated at QCISD(T)/6-311+G(d,p) level of theory are presented in Table 1. We have used the M062X/BS1 energetics and geometric parameters in successive discussions unless otherwise mentioned.

In VA, there are different chemical environments for the H atom linked with C1, C3, and C4 carbon atoms. For all H-atom abstraction channels, the infinitely separated reactants directly transform into the transition state without forming any prereactive complexes.

H-Atom Abstraction from C1. As shown in Figure 1, the heavy atoms of VA are in plane and there is a C1–C2 free rotation; thus, there are two types of chemical environment present for the H-atoms linked with C1, e.g., one is in plane and other is out of plane of the heavy atoms. The in-plane H-atom is abstracted by the OH radical via the transition state TSC1-P located at a 2.75 kcal mol⁻¹ higher point than the reactant in the PES. In TSC1-P, the OH radical also exists on the plane of heavy atom containing the breaking C–H and forming O–H bonds with distances 1.21 and 1.29 Å, respectively. The OH radical can also abstract the out-of-plane H-atoms through the transition state TSC1 with 2.87 kcal

mol⁻¹ barrier of activation. The aforementioned two H-abstraction channels produce the same product, P1-(\bullet CH₂COOCHCH₂).

H-Atom Abstraction from C4. There are two types of H atoms of C4 situated in slightly different chemical environments. As this type of H-abstraction is not so important for the title reaction, only one abstraction channel is presented here. The product P2 is formed via the transition state TSC4 which possesses 4.92 kcal mol⁻¹ energy of activation. In TSC4, there is a possibility of H-bonding stabilization between the central O atom of VA and the H atom of the OH radical. From the calculation it is clear that the energy barrier for H-atom abstraction from C4 is almost 2.80 kcal mol⁻¹ higher than H-atom abstraction from C1.

H-Atom Abstraction from C3. There is only one H-atom linked with C3 in VA, and it is abstracted via the transition state TSC3 containing 6.73 kcal mol⁻¹ barrier of activation. Comparing the entire H-atom abstraction channels, we can arrange them in the order of preference, C1 > C4 > C3, which can be explained by the stability order of the product radicals.

Addition Reaction Pathways. The initial OH addition of VA is performed via the electrophilic addition to the π system due to the electrophilic nature of OH radical. In VA, there are two sites of attack for OH leading to two different radical intermediates, IM1 and IM2. The related optimized geometries with geometrical parameters are presented in Figure 1, and Figure 2 shows the M062X/BS1 PES for the addition reactions. The necessary energetics parameters are collected in Table 1.

The OH radical approaches VA to form a weakly bound complex, RC, through a barrierless path, which is 4.94 kcal mol⁻¹ more stable than the separated reactants. It is important to mention here that RC is the precursor adduct complex that leads to the formation of both IM1 and IM2. In RC, the distances between oxygen atom of the OH radical and terminal and internal carbon atoms of VA are 3.16 and 2.85 Å, respectively. The transition states involved in the formation of IM1 and IM2 exist below the separated reactants. This fact (reaction with negative barrier height) can clearly be established from the kinetics analysis which shows negative temperature dependence of the rate coefficient. Our theoretical treatment of kinetics (discussed later), which is in good agreement with the experimental results, also establishes the same fact.

RC → IM1. This pathway, essentially an addition of OH radical to the terminal carbon of the π system, proceeds from RC via the transition state, TS1 which is 1.61 kcal mol⁻¹ below the energy of the separated reactants. In TS1, the forming C–OH distance is 2.16 Å. TS1 contains an imaginary frequency of 334.6 cm⁻¹, and the transition vector for this mode corresponds mainly to the shuttle of OH group to the carbon atom of the VA. The TS1 then produces the radical intermediate IM1, which is situated 29.62 kcal mol⁻¹ lower than the energy of the separated reactants VA + OH. In IM1, the formed C–O distance is 1.42 Å, which is close to the normal C–O single bond length.

RC → IM2. This reaction channel proceeds from RC through the internal attack of OH radical that produces the radical intermediate IM2 via the transition state TS2. Like TS1, TS2 is also 1.27 kcal mol⁻¹ lower in energy than the separated reactants. The forming bond length C–O in TS2 is 2.11 Å. The imaginary vibrational frequency of 366.3 cm⁻¹ is due to the OH approaching transition vector from infinite separation to the internal carbon of π moiety of the VA. Finally, after TS2, IM2 is

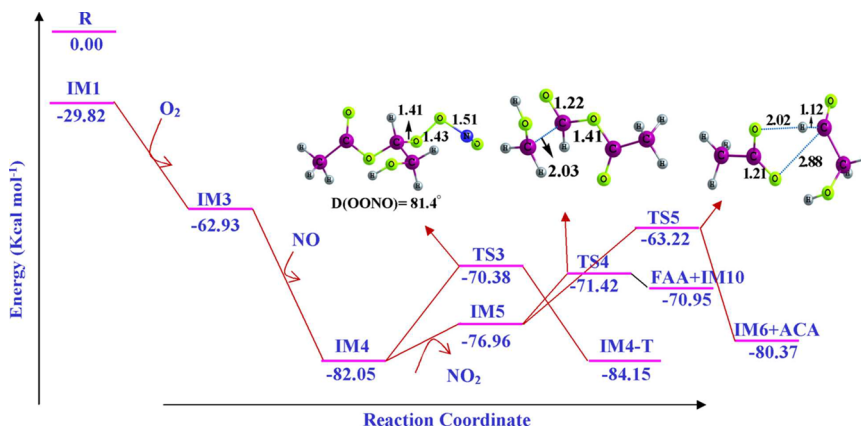


Figure 3. M062X/BS1 calculated potential energy (ZPVE corrected) profile for the subsequent reaction pathways of IM1 in presence O_2 and NO.

formed through a reaction that is 36.16 kcal mol⁻¹ exothermic. IM2 is 6.64 kcal mol⁻¹ more stable than IM1, which is due to the formation of H-bond through the OH···O(1) of VA with the interaction distance 2.16 Å. For the proof of H-bond stabilization, we have carried out Bader's atoms in molecules analysis. The molecular graphs of IM1 and IM2 of Figure S1 presented in the Supporting Information show clearly the presence of H-bond interaction in IM2. On the other hand, no such H-bonding stabilization factor is present in IM1. In IM2, the formed C–O bond distance is 1.38 Å which is slightly lower (0.04 Å) than that in IM1.

It is of further interest to compare the formation of IM1 and IM2. IM1 is formed through lower barrier height than IM2, but IM2 possesses higher exothermicity. Owing to these facts, we can say that IM1 is the kinetically favorable product and IM2 is the thermodynamically favorable one. From the negative barrier height and higher exothermicity, it can be concluded that the radical addition to π moiety is extremely plausible.

Atmospheric Reaction Pathways of IM1 and IM2. The mechanism for the OH-initiated oxidation of VA is very extensive, involving not only the generation of the radical intermediate by OH addition but also any relevant chemical reactions that occur subsequently in the atmosphere. It is worth mentioning here that IM1 and IM2 are produced through exothermic pathways, and consequently there are possibilities for unimolecular reactions, e.g., isomerization or decompositions from the radical intermediates IM1 and IM2 formed initially. From previous experimental product detection study,¹⁰ it is observed that there is no favorable isomerization or decomposition reaction. So the reaction of IM1 and IM2 in the presence of O_2 and NO is the only dominant reaction channel and responsible for the ultimate fate of the reactant.

Reaction of IM1 with O_2 and NO. Now we consider the degradation process of IM1, a new radical formed by the terminal addition of OH, in the reaction with O_2 and NO. In the first pathway the ubiquitous O_2 will be added to IM1 through the attack of the neighboring carbon atom of the OH-linked carbon from the opposite side and produces hydroxyperoxy radical IM3 [$CH_3C(O)OCH(O^{\bullet}O)CH_2OH$]. The M06-2X/BS1 optimized structures of the species are displayed in Figure 1 with their respective geometrical parameters. Figure 3 depicts the M062X/BS1 PES for the decomposition of IM1 by the reaction of O_2 followed by NO.

This addition process occurs without any transition state. The scan of relaxed potential energy surface presented in Figure S2 in the Supporting Information further clarifies that there is

no transition state for the O_2 addition. IM3 is produced through an exothermic addition of O_2 with 33.11 kcal mol⁻¹ lower in energy than the sum of energies of IM1 and O_2 .

Now in atmospheric conditions the IM3 reacts with NO to form a cis ONOO configuration intermediate IM4 [$CH_3C(OONOO)CH_2OH$]. This addition process is exothermic and barrierless. IM4 lies 19.12 kcal mol⁻¹ lower in energy than the sum of energies of the reactants. The cis IM4 can also be transformed into the more stable trans IM4-T configuration, which is about 2 kcal mol⁻¹ more stable than the cis conformation. There is a rotational transition state, TS3, with 11.7 kcal mol⁻¹ barrier of activation between cis and trans conformers. The imaginary frequency 198.2 cm⁻¹ is due to the rotational transition vector for the –ONO fragment. Very high reaction energy of 52.28 kcal mol⁻¹ in the two consecutive processes is preserved because of the internal energy of IM4 which makes it easier to overcome the potential barrier for the successive reactions.

From IM4 and IM4-T, with the release of NO_2 , an alkoxy radical IM5 [$CH_3C(O)C(O^-)HCH_2OH$] is formed. The radical intermediate IM5 is a vital species in the decomposition PES, as it is one of the important precursors for the production of two identified major products, formic acetic anhydride (FAA) and acetic acid. From IM5, there are two possibilities for the successive reaction paths; it may be decomposed or rearranged to produce formic acetic anhydride and acetic acid, respectively.

The decomposition of IM5 occurs via a transition state TS4 with a barrier of activation of 5.54 kcal mol⁻¹. In TS4, the breaking C–C bond length increases 0.47 Å from the reactant IM5. The TS4 contains an imaginary vibrational frequency of 367.4 cm⁻¹ responsible for the stretching of the C–C bond. After complete breakage of the C–C bond, TS4 then generates two products; one is the major oxidation product of VA, the FAA, and the other is the radical intermediate IM10 ($^{\bullet}CH_2OH$).

The primary formation of the acetic acid can be explained by the second possible route for IM5, a rearrangement called the α -ester rearrangement occurring by an H-atom transfer through a five-member ring transition state TSS. This type of rearrangement responsible for the ester oxidation processes has also been observed for other acetates and propionates.^{16–18,44} The activation energy of TSS is 8.20 kcal mol⁻¹ higher than that of the TS4, making the rearrangement less important than the decomposition. Owing to this fact, it is established that FAA is the major oxidation product that

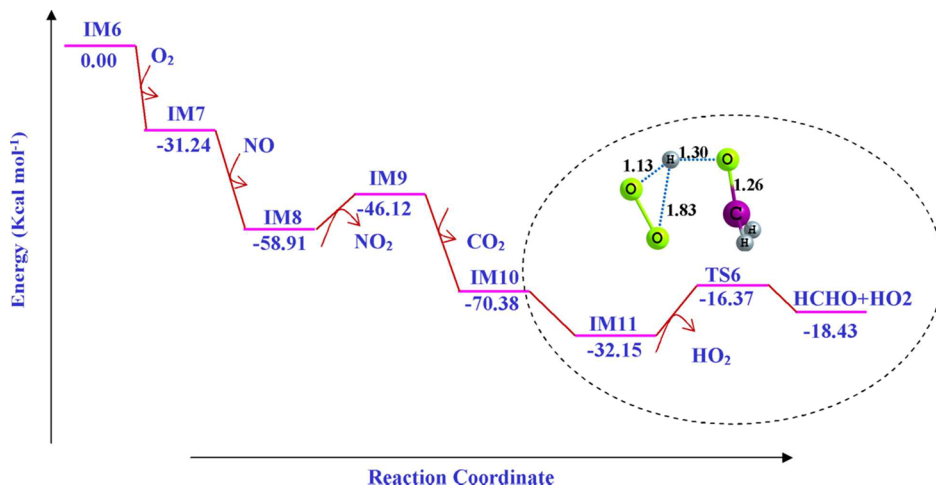


Figure 4. M062X/BS1 calculated potential energy (ZPVE corrected) profile for the subsequent reaction pathways of IM6 in presence O_2 and NO. The surface enclosed by the circle is drawn with reference to IM10.

supports the experimental observation. TS5 is a five-member ring containing transition state in which the forming O–H and the breaking O–C bond distances are 2.03 and 3.03 Å, respectively. Moreover, TS5 is a product-like or late transition state because in the transition state geometry the O–C bond breaks almost completely and the forming O–H bond distance decreases 0.43 Å from that in the reactant. In TS5, an imaginary frequency 150.5 cm^{-1} is responsible for the shuttle of proton from the carbon to carbonyl oxygen as well as the breakage of the O–C bond transition vector. The IM6 ($\text{OH}-\text{CH}_2\text{CO}^\bullet$) radical intermediate, which is produced simultaneously by this channel, can react with O_2 and NO for further decomposition.

Reaction of IM6 with O_2 and NO. To explore all the reactions of IM6 in the atmosphere, the mechanism has been investigated in detail. The degradation mechanism of IM6 proceeds in a similar way like IM1. For better understanding of the reaction mechanism and to avoid complexity, we draw another PES, shown in Figure 4, with respect to the reference energy of IM6.

The required geometries with geometrical parameters are depicted in Figure 1. Once formed in the atmosphere, the radical intermediate IM6 reacts with O_2 and produces IM7 ($\text{HO}-\text{CH}_2\text{C}(\text{O})\text{OO}^\bullet$). It is important to mention here that no possible unimolecular or hydrogen abstraction channel is observed for IM6. The hydroxy-peroxyacetyl nitrate (hydroxy-PAN), which is a transient species and was not identified in the previous spectroscopic product detection study, may be produced after the addition reaction of NO_2 with IM7. Therefore, we would not concentrate on this. The abandoned O_2 is added to the vicinal carbon atom of the OH group without any extra barrier through a strongly exothermic path. IM7 is situated at 31.24 kcal mol⁻¹ lower energy point in the PES than the sum of the energies of IM6 and NO.

Now IM7 is ready to react with NO for abstraction of one oxygen atom. Like IM1, the addition of NO to IM7 is barrierless and strongly exothermic. After the addition of NO, the intermediate IM8 [$\text{HO}-\text{CH}_2-\text{C}(\text{O})\text{OONO}$] lies 27.67 kcal mol⁻¹ lower in energy than the sum of energies of IM7 and NO.

From IM8, the IM9 [$\text{HO}-\text{CH}_2\text{C}(\text{O})\text{O}^\bullet$], which is the precursor radical of formaldehyde, is produced after the loss of NO_2 by O–O bond fission in IM8. The elimination of NO_2 also occurred without any barrier, and IM9 lies at 12.21 kcal

mol^{-1} higher energetic point in the PES. After generation of IM9, it further eliminates CO_2 with the production of IM10 (${}^*\text{CH}_2\text{OH}$) which may also be produced from the decomposition reaction channel of IM5 as a co-product of FAA. CO_2 is also an identified product of the atmospheric oxidation of VA.

In the presence of O_2 the IM10 reacts further to produce the ultimate products HCHO and HO_2^\bullet radical, and it may be possible through two different ways, the first one being the direct H-abstraction from –OH group by O_2 . From early research²⁰ in this field, it was found that this abstraction channel proceeded through an activation barrier of 15.80 kcal mol⁻¹. The second possibility, the pathways for the generation of final product, is the addition of O_2 to the carbon atom of the IM10, producing IM11 [$\text{HOCH}_2(\text{OO})$], followed by the H-shift from –OH group to O_2 and subsequent cleavage of the C–O bond. The H-shuttle and C–O bond cleavages occurred via the transition state TS6 with a barrier height of 15.78 kcal mol⁻¹. This value is well harmonized with the previously reported result. Another important fact to mention here is that we could not find any preproduct complex in this step as reported by the earlier study.²⁰ TS6 is a five-member transition state in which the shifting H-atom is located almost at the center of the two oxygen atoms, and the breaking C–O bond distance increases by 0.45 Å from that of the reactant, IM11. The addition of O_2 will occur through a complete barrierless and extreme exothermic pathway with the release of 38.23 kcal mol⁻¹ energy. So at this time the system has sufficient internal energy to cross the subsequent potential barrier. Therefore, one can state that the addition and decomposition will be the energetically more favorable pathway for the formation of HCHO + HO_2 than the direct H-abstraction pathway.

From the above analysis it can be established that the FAA, acetic acid, peroxy radical HO_2 , and formaldehyde are the major products obtained from the reaction of IM1 in the presence of O_2 and NO. Finally, we can state that our computational approach is successful to predict all the product generation mechanisms which are further corroborated with the outcome of the experimental study of the detection of products.

Reaction of IM2 with O_2 and NO. Like IM1, the atmospheric reactions of IM2 with O_2 and NO also occur in a similar way. The geometries of the associated species with

structural parameters are displayed in Figure 5, and the M062X/BS1 potential energy profile is presented in Figure 6.

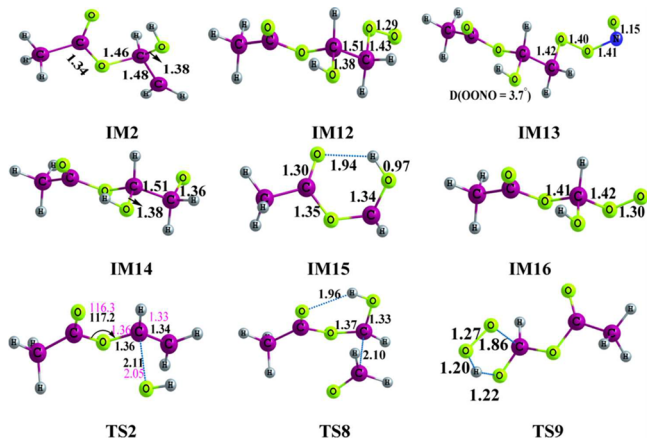


Figure 5. Optimized geometries with geometrical parameters calculated at M06-2X/BS1 level for all the species involved in the internal OH-initiated oxidation of vinyl acetate in presence of O_2 and NO addition reaction.

The atmospheric reaction of IM2 is started with the addition of O_2 at the terminal carbon atom. For the addition of O_2 , no transition state is located and IM12 [$CH_3C(O)OCH(OH)-CH_2OO^\bullet$] is produced via an exothermic process with release of 31.92 kcal mol⁻¹ energy. In IM12, the newly formed C–O bond distance is 1.43 Å.

There is a possibility of addition of NO_2 to the IM12 for the generation of hydroxy-peroxyacetyl nitrate type compound, but the addition of NO is energetically more favorable. Therefore, we consider further the reaction of IM12 with NO. The NO is added to IM12 without any barrier as well as through an energy releasing process and produces IM13 [$CH_3C(O)OCH(OH)-CH_2OONO$] which lies at 19.63 kcal mol⁻¹ lower point in the respective PES. In IM13, the –OONO group is linked terminally and there is no steric effect; therefore, the energy will slightly depend on the orientation of the –OONO group.

Now IM13 produces an alkoxy radical IM14 [$CH_3C(O)-CH(OH)CH_2O^\bullet$] after elimination of NO_2 group. IM14 then decomposes with the breaking of C–C bond to produce formaldehyde and the precursor radical of FAA. This disintegration occurs via the transition state TS7 with a barrier height of 12.62 kcal mol⁻¹. It contains an imaginary frequency

288.7 cm⁻¹ which is due to the stretching of the breakable C–C bond. In TS7, the disintegrating C–C bond distance increases by 0.59 Å from that in IM14. TS7 then transforms into a complex containing IM15 [$CH_3C(O)OC(\cdot)H(OH)$] and HCHO with –34.44 kcal mol⁻¹ energy with respect to IM2.

Like IM10, in IM15 there is also a probability of H-abstraction by O_2 to form the target product FAA. This high energy barrier pathway is not analyzed here, but the favorable pathway in the atmosphere, the addition/elimination pathway, is discussed here. So O_2 is added to the unpaired electron containing carbon atom of the IM15 to generate IM16 [$CH_3C(O)OCH(OH)OO^\bullet$] with an exothermic and barrierless channel. One H atom is shifted from the OH group to the terminal O atom of the newly added O_2 , followed by the breaking of the C–O bond in the transition state TS8. TS8 possesses an imaginary frequency 899.90 cm⁻¹; such a high frequency is mainly due to the transformation of H-atom. Finally, after release of the HO_2 radical, the target product FAA will be produced.

As a summary of the above section, we can say that FAA may be produced from both IM1 and IM2 in the presence of O_2 and NO. For the IM1 reaction channel, the precursor radical for FAA is IM5 and in case of the IM2 decomposition path, it is the IM16. IM5 is the only radical responsible for the generation of acetic acid. Formaldehyde is produced through a number of mechanistic pathways. Lastly, a few radicals are also freed in the atmosphere, e.g., HO_2 and CO_2 are also produced as co-products of HCHO from IM9. Therefore, our present theoretical calculation is sufficient for the justification of the products surveyed by the experiment.

Thermochimistry. All the reactants, reactive intermediates, and products involved in the reaction of OH-initiated oxidation of VA are important, as they are released in the troposphere. So thermochemical analysis is essential for the identification and determination of the stability of the species. In this article we have computed the most important thermochemical parameter, namely, the standard enthalpies of formation at 298.15 K ($\Delta_f H^\circ_{298.15}$) using CBS–QB3 electronic energies, and the results are collected in Table 2.

The high-accuracy energy prediction model CBS–QB3 is tested well for the related species and is reported to produce very accurate enthalpy of formation values. As there is a lack of experimental or previous theoretical information on $\Delta_f H^\circ_{298.15}$ for most of the species involved in this study, the accuracy of the method is verified by comparing the calculated enthalpy of

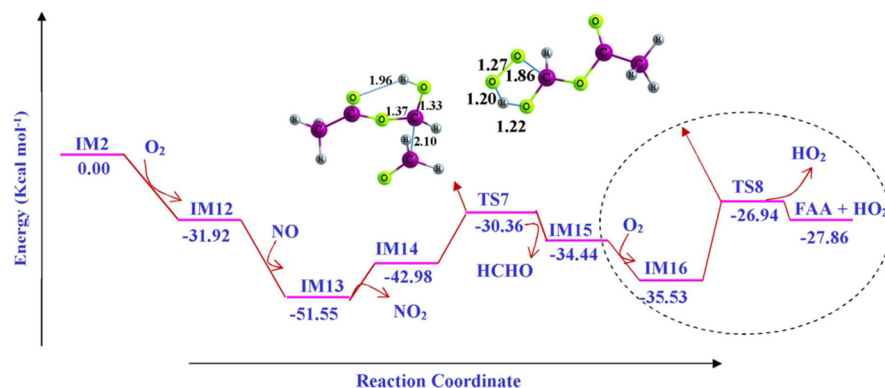


Figure 6. M062X/BS1 calculated potential energy (ZPVE corrected) profile for the subsequent reaction pathways of IM6 in presence O_2 and NO. The surface enclosed by the circle is drawn with reference to IM15.

Table 2. Standard Enthalpies of Formation at 298.15 K Calculated Using CBS–QB3 Energies for All the Species Involved in the OH-Initiated Oxidation of Vinyl Acetate in Presence of O₂ and NO

species	$\Delta_f H^\circ_{298.15}$	expt	species	$\Delta_f H^\circ_{298.15}$	expt
OH	9.13	8.93 ^a	IM9	-73.43	
O ₂	0.21	0.0 ^b	IM10	-3.30	-2. ± 1 ^f
NO	-37.8		IM11	-38.74	
CO ₂	-94.88	-94.05 ^c	IM12	-135.53	
HO ₂	2.93	0.5 ^c	IM13	-199.27	
H ₂ O	-57.72	-57.79 ^c	IM14	-134.78	
HCHO	-26.36	-27.7 ^c	IM15	-92.46	
CH ₃ COOH	-102.65	-103.5 ^d	IM16	-72.16	
FAA	-124.91		TS1	-68.19	
VA	-73.78	-73.8 ^e	TS2	-68.45	
RC	-68.75		TSC1-P	-63.01	
IM1	-94.07		TSC1	-106.90	
IM2	-100.96		TSC4	-60.97	
P1	-27.34		TSC3	-97.82	
P2	-11.63		TS3	-182.50	
P3	-13.18		TS4	-128.79	
IM3	-130.36		TSS	-123.72	
IM4	-193.86		TS6	26.63	
IM4-T	-195.05		TS7	-124.25	
IM5	-132.85		TS8	-124.81	
IM6	-34.90				
IM7	-68.25				
IM8	-140.36				

^aReference 51. ^bReference 52. ^cReference 53. ^dReference 54. ^eReference 55. ^fReference 56

formation values with the existing literature for VA, OH, O₂, HCHO, CH₃COOH, etc., and good agreement is observed (refer to Table 2). We have also calculated the $\Delta_f H^\circ_{298.15}$ values for the transition states involved in the title reaction.

Kinetics. In the present work we have explored the kinetics of the gas-phase reactions of OH radical with VA. The title reaction is one of the important radical–molecule reactions in the troposphere. From the analysis of energetics of the H-abstraction and OH-addition reactions, it is obvious that the addition reaction is favored.

As the attack of OH radical on VA forms a prereactive complex, shown in Figure 2, we can assume that the reaction occurs according to the following two-step mechanism:



The first step involves a fast pre-equilibrium between the reactants and reaction complex, and the second step is the addition of OH to VA. As the OH radical is highly reactive to VA and the reaction proceeds without any energy obstacle, the formation of the fast pre-equilibrium in the initial step may be justified. This pre-equilibrium step is also responsible for the negative temperature dependence of the rate constants, as at high temperature the probability of formation of the weakly bound complexes decreases which lowers the rate.

If k_1 and k_{-1} are the forward and reverse rate constants for the first step and k_2 is that for the second step, after steady state analysis, the effective rate constant can be calculated by the following equation:

$$k_{\text{tot}} = \frac{k_1 k_2}{k_{-1} + k_2}$$

Assuming $k_2 \ll k_{-1}$, the above equation can be written as

$$k_{\text{tot}} = \frac{k_1}{k_{-1}} k_2$$

$$k_{\text{tot}} = k_{\text{eq}} k_2$$

where k_{eq} is the equilibrium constant of the first step. k_{eq} can be estimated by basic statistical thermodynamic equation

$$k_{\text{eq}} = \sigma_{\text{eq}} \left(\frac{Q_{\text{RC}}}{Q_{\text{OH}} Q_{\text{VA}}} \right) \exp \left(- \frac{E_{\text{RC}} - E_{\text{OH}} - E_{\text{VA}}}{k_b T} \right)$$

where Q_{OH} and Q_{VA} are the partition functions for the reactants and Q_{RC} is that for the prereactive complex. E_{RC} , E_{OH} , and E_{VA} denote the total energy (ZPVE corrected) of the prereactive complex, OH, and VA, respectively. The constant σ is the symmetry factor counting the number of possible identical reaction paths. As VA possesses C_s point group symmetry, it has two equal probable faces for the attack of OH radical. As a result, the reaction symmetry number 2 is chosen here for the first step. The k_b and T are the Boltzmann constant and the absolute temperature, respectively. The rate for the second step can be evaluated using the conventional TST equation

$$k = \kappa \sigma \frac{k_b T}{h} \left(\frac{Q_{\text{TS}}}{Q_{\text{RC}}} \right) \exp \left(- \frac{E_{\text{TS}} - E_{\text{RC}}}{k_b T} \right)$$

where Q_{TS} and E_{RC} are the partition function and energy of the transition state, respectively, and κ is the tunneling factor that originates from quantum mechanical tunneling through the potential energy barrier along the reaction coordinate.

The kinetics calculations have been carried out at 1 atm pressure. The approach adopted here is good enough for the calculation of rate constants at high pressure limit, as the formation of first prereactant complex is favored at high pressure. In our calculation this approach also shows a good

performance. So we can say that at 1 atm pressure the results for the kinetics are expected to be fairly close to that for the high pressure limit.

As the two addition reactions occur via one reactant complex, the second step can be treated as a parallel reaction and we get two rate constants for the second step, k_{ter} for the terminal and k_{in} for the internal. The total rate constant will be a sum of the two.

$$k_{\text{tot}} = k_{\text{ter}} + k_{\text{in}}$$

For the H-atom abstraction pathways, as the prereactive complexes have no effect, the free energy difference between TS and separated reactants should reflect the real kinetics and the rate constant can be calculated by the conventional TST equation. The kinetics calculations have been carried out using M06-2X energetics parameters. The rate constants at 298 K for the H-abstraction channels are 3.62×10^{-15} , 2.80×10^{-16} , and $9.53 \times 10^{-18} \text{ cm}^3 \text{ molecule}^{-1} \text{ s}^{-1}$ from C1, C4, and C3 carbon atoms, respectively.

All kinetic calculations have been performed using the TheRate program.⁴⁵ In these calculations, overall rotations are treated classically and vibrations are treated quantum mechanically within the harmonic approximation except for the modes corresponding to the internal rotations of the CH₃ groups which are treated as hindered rotations using the method of Ayala et al.⁴⁶

The corrections for quantum mechanical tunneling have been taken into account by unsymmetrical Eckart's formalism.⁴⁷ The rate coefficients obtained by this procedure, which was applied to previous investigations^{48–50} also, show a good agreement with the reported experimental values.

The rate constant for the terminal addition are found to be slightly higher than that for the internal addition; this may be due to the repulsion of OH radical by the O(2) atom of VA.

The Arrhenius fitted rate constants (k_{tot}) for the addition reactions along with the experimental rates have been presented in Figure 7. The standard least-squares procedure has been applied to calculate the Arrhenius fitted rate parameters. The rate coefficient data measured at 298 K and 1 atmospheric pressure for the addition part of the title reaction can be presented as

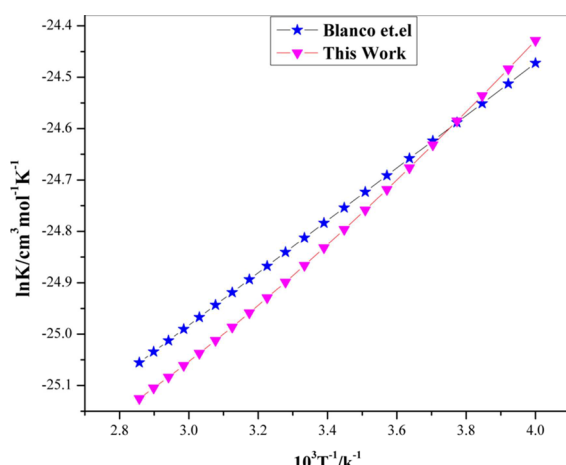


Figure 7. Arrhenius fitted rate constants for the OH addition reactions along with the experimental data.

$$k_{298\text{K}} = (2.48 \pm 0.61) \times 10^{-11} \text{ cm}^3 \text{ molecule}^{-1} \text{ s}^{-1}$$

(Blanco et al.¹¹)

$$k_{298\text{K}} = (2.3 \pm 0.3) \times 10^{-11} \text{ cm}^3 \text{ molecule}^{-1} \text{ s}^{-1}$$

(Picquet-Varrult et al.¹⁰)

$$k_{298\text{K}} = 1.61 \times 10^{-11} \text{ cm}^3 \text{ molecule}^{-1} \text{ s}^{-1} \quad (\text{our work})$$

It is worth mentioning here that the rates of the abstraction channels with respect to addition channels are negligible; therefore, the branching ratio is not so sensitive to the reaction pathways and addition rate represents almost the overall rate of the reaction. The computed rate constant in our study shows good agreement with the experimental values.

The rate constants for the addition reaction in the temperature range 250–350 K are given in Table S1 in the Supporting Information. From those values we see that the rate constant decreases with the increasing temperature. It can be explained from the first pre-equilibrium step, as with rising temperature the rate of the reverse process increases which lowers the value of the equilibrium rate constant. It is also observed from Figure 7 that the Arrhenius plots become upward with decreasing temperature.

Although our predicted result agrees to a good proportion with the established experimental values, there is small deviation in the absolute values. This can be attributed to the theoretical limitation of the barrier height calculation and corresponding rate constant estimated by transition state theory. This deviation is negligibly small, as the computed rate constants are not affected much by such energy errors in the adduct-forming reactions where the prereaction complexes are just formed by noncovalent interactions. Since this step of formation of prereaction complex is the rate determining step, we can partially ignore the errors that may be generated from the barrier height calculation. But the trends (Figure 7) and most importantly the negative temperature dependent rate coefficients are clearly established by this approach.

Hence, from the above kinetics analysis we can claim that the trends in the reaction rate obtained from the present work are well harmonized with the experimental findings, without paying too much attention to the absolute values of rate constants.

CONCLUSION

In the present theoretical study, quantum chemical methods and reaction kinetics theories are applied to investigate the OH-initiated atmospheric degradation of vinyl acetate. We have explored the chemical kinetics for the reactions of the OH radical with VA and constructed a global potential energy surface to understand the reaction mechanism comprehensively. The main calculations have been performed using the M06-2X density functional method of Truhlar et al., developed specifically for the kinetic studies. The conventional transition state theory calculations on radical additions of the bimolecular reactions have been performed to explain the experimentally observed trends of the rate coefficients with temperature.

The reactions are initiated by an addition of OH to the less and more substituted ethylenic C-atoms of VA with a negative entrance barrier. The H-abstraction channels possess very high energetics than the addition. Consequently, the addition reaction is almost exclusive and passes through a prereactive complex. The addition processes are found to be exothermic, and the transition states lie below the separated reactants. The

overall rate constants for this reaction calculated at 298 K and 1 atm pressure are close to the order of $10^{-11} \text{ cm}^3 \text{ molecule}^{-1} \text{ s}^{-1}$. Our theoretical calculation is also well harmonized with the experimental results (numerical values for rate constants are given in the Supporting Information). The non-Arrhenius behavior of the VA + OH[•] reaction has been elucidated in the present study. The addition processes give rise to two isomeric adducts IM1 and IM2, which is consistent with the experimental observations. Under atmospheric conditions, O₂ can react with two adducts IM1 and IM2 before their unimolecular rearrangement or decomposition.

The oxidation products are analyzed thermochemically by calculating their standard enthalpies of formation at 298.15 K ($\Delta H^\circ_{298.15}$). Our computations first provide the mechanistic and kinetics of the atmospheric oxidation of an ester (VA) compound. Most significantly the mechanism proposed in this article can explain the experimentally observed products, formic acetic anhydride, acetic acid, and formaldehyde. Since VA is an important tropospheric pollutant and the main daytime oxidative degradation of VA occurred by the reaction with OH radical, the mechanistic and kinetic information given in this work is essential in order to fully understand the tropospheric chemistry of VA as well as its subsequent fate.

■ ASSOCIATED CONTENT

S Supporting Information

Rate parameters at different temperature, Cartesian coordinates for optimized geometries, ZPVE, thermochemical parameters, imaginary frequencies of the transition states, moments of inertia, and symmetry factor for all the species. This material is available free of charge via the Internet at <http://pubs.acs.org>.

■ AUTHOR INFORMATION

Corresponding Author

*E-mail: spakd@iacs.res.in.

Notes

The authors declare no competing financial interest.

■ ACKNOWLEDGMENTS

D.M and C.S. are very grateful to the Council of Scientific and Industrial Research (CSIR), Government of India, for providing Research Fellowships. S.B. is thankful to NSEC, Kolkata, India, for allowing him to work at Indian Association for the Cultivation of Science. Thanks also are due to the reviewers for their valuable suggestions.

■ REFERENCES

- (1) Graedel, T. E.; Hawkins, D. T.; Claxton, L. D. *Atmospheric Compounds: Sources, Occurrence, and Bioassay*; Academic Press: Orlando, FL, 1986.
- (2) Koppmann, R., Ed. *Volatile Organic Compounds in the Atmosphere*; Wiley-Blackwell: New York, 2007.
- (3) Organization for Economic Co-Operation and Development, OECD Integrated HPV Database. <http://www.oecd.org/>.
- (4) Calvert, J. G.; Derwent, R. G.; Orlando, J. J.; Tyndall, G. S.; Wallington, T. J. *Mechanisms of Atmospheric Oxidation of the Alkanes*; Oxford University Press: New York, 2008.
- (5) Calvert, J. G.; Atkinson, R.; Kerr, J. A.; Madronich, S.; Moortgat, G. K.; Wallington, T. J.; Yarwood, G. *The Mechanisms of Atmospheric Oxidation of the Alkenes*; Oxford University Press: New York, 2000.
- (6) Calvert, J. G.; Atkinson, R.; Becker, K. H.; Kamens, R. M.; Seinfeld, J. H.; Wallington, T. J.; Yarwood, G. *The Mechanisms of Atmospheric Oxidation of the Aromatic Hydrocarbons*; Oxford University Press: New York, 2002.
- (7) Hodgson, A. T.; Wooley, J. D.; Daisey, J. M. Emissions of Volatile Organic Compounds from New Carpets Measured in a Large-Scale Environmental Chamber. *J. Air Waste Manage. Assoc.* **1993**, *43*, 316–323.
- (8) *Toxic Chemical Release Inventory*; Office of Toxic Substances, U.S. Environmental Protection Agency: Washington, DC, 2006; <http://toxnet.nlm.nih.gov/cgi-bin/sis/htmlgen/TRI.htm>.
- (9) Mellouki, A.; Le Bras, G.; Sidebottom, H. Kinetics and Mechanisms of the Oxidation of Oxygenated Organic Compounds in the Gas Phase. *Chem. Rev.* **2003**, *103*, 5077–5096.
- (10) Picquet-Varrault, B.; Scarfogliero, M.; Doussin, J. F. Atmospheric Reactivity of Vinyl Acetate: Kinetic and Mechanistic Study of Its Gas-Phase Oxidation by OH, O₃, and NO₃. *Environ. Sci. Technol.* **2010**, *44*, 4615–4621.
- (11) Blanco, M. B.; Bejan, I.; Barnes, I.; Wiesen, P.; Teruel, A. M. OH-Initiated Degradation of Unsaturated Esters in the Atmosphere: Kinetics in the Temperature Range of 287–313 K. *J. Phys. Chem. A* **2009**, *113*, 5958–5965.
- (12) Grosjean, E.; Grosjean, D. Rate Constants for the Gas-Phase Reaction of Ozone with Unsaturated Oxygenates. *Int. J. Chem. Kinet.* **1998**, *30*, 21–29.
- (13) Blanco, M. B.; Taccone, R. A.; Lane, S. I.; Teruel, M. A. On the OH-Initiated Degradation of Methacrylates in the Troposphere: Gas-Phase Kinetics and Formation of Pyruvates. *Chem. Phys. Lett.* **2006**, *429*, 389–394.
- (14) Blanco, M. B.; Teruel, M. A. Photodegradation of Butyl Acrylate in the Troposphere by OH Radicals: Kinetics and Fate of 1,2-Hydroxyalcoxy Radicals. *J. Phys. Org. Chem.* **2008**, *21*, 397–401.
- (15) Atkinson, R.; Baulch, D. L.; Cox, R. A.; Crowley, J. N.; Hampson, R. F.; Hynes, R. G.; Jenkin, M. E.; Rossi, M. J.; Troe, J. Evaluated Kinetic and Photochemical Data for Atmospheric Chemistry: Volume II. Gas Phase Reactions of Organic Species. *Atmos. Chem. Phys.* **2006**, *6*, 3625–4055.
- (16) Tuazon, E. C.; Aschmann, S. M.; Atkinson, R.; Carter, W. P. L. The Reactions of Selected Acetates with the OH Radical in the Presence of NO: Novel Rearrangement of Alkoxy Radicals of Structure RC(O)OCH(Ö)R. *J. Phys. Chem. A* **1998**, *102*, 2316–2321.
- (17) Christensen, L. K.; Ball, J. C.; Wallington, T. J. Atmospheric Oxidation Mechanism of Methyl Acetate. *J. Phys. Chem. A* **2000**, *104*, 345–351.
- (18) Picquet-Varrault, B.; Doussin, J. F.; Durand-Jolibois, R.; Carlier, P. FTIR Spectroscopic Study of the OH-Induced Oxidation of Two Linear Acetates: Ethyl and n-Propyl Acetates. *Phys. Chem. Chem. Phys.* **2001**, *3*, 2595–2606.
- (19) Galano, A. Theoretical Study on the Reaction of Tropospheric Interest: Hydroxyacetone + OH. Mechanism and Kinetics. *J. Phys. Chem. A* **2006**, *110*, 9153–9160.
- (20) Du, B.; Zhang, W. Theoretical Mechanistic Study of OH-Initiated Atmospheric Oxidation Reaction of Allyl Alcohol in the Presence of O₂ and NO. *Comput. Theor. Chem.* **2011**, *977*, 111–122.
- (21) Galano, A.; Alvarez-Idaboy, J. R.; Ruiz-Santoyo, M. E.; Vivier-Bunge, A. Glycolaldehyde + OH Gas Phase Reaction: A Quantum Chemistry + CVT/SCT Approach. *J. Phys. Chem. A* **2005**, *109*, 169–180.
- (22) Galano, A.; Alvarez-Idaboy, J. R.; Bravo-perez, G.; Ruiz-Santoyo, M. E. Gas Phase Reactions of C₁–C₄ Alcohols with the OH Radical: A Quantum Mechanical Approach. *Phys. Chem. Chem. Phys.* **2002**, *4*, 4648–4662.
- (23) Galano, A.; Alvarez-Idaboy, J. R. In *Applications of Theoretical Methods to Atmospheric Science*; Sabin, J. R., Brändas, E., Eds.; Advances in Quantum Chemistry, Vol. 55; Elsevier: Boston, MA, 2008, p 245.
- (24) Alvarez-Idaboy, J. R.; Mora-Diez, N.; Boyd, R. J.; Vivier-Bunge, A. On the Importance of Prereactive Complexes in Molecule–Radical Reactions: Hydrogen Abstraction from Aldehydes by OH. *J. Am. Chem. Soc.* **2001**, *123*, 2018–2024.
- (25) Francisco, J. S.; Eisfeld, W. Atmospheric Oxidation Mechanism of Hydroxymethyl Hydroperoxide. *J. Phys. Chem. A* **2009**, *113*, 7593–7600.

- (26) Alvarez-Idaboy, J. R.; Cruz-Torres, A.; Galano, A.; Ruiz-Santoyo, M. E. Structure-Reactivity Relationship in Ketones + OH Reactions: A Quantum Mechanical and TST Approach. *J. Phys. Chem. A* **2004**, *108*, 2740–2749.
- (27) Christiansen, C. J.; Francisco, J. S. Atmospheric Oxidation of Trichloroethylene: An Ab Initio Study. *J. Phys. Chem. A* **2010**, *114*, 9163–9176.
- (28) Zhao, Y.; Truhlar, D. G. The M06 Suite of Density Functionals for Main Group Thermochemistry, Thermochemical Kinetics, Non-covalent Interactions, Excited States, and Transition Elements: Two New Functionals and Systematic Testing of Four M06-Class Functionals and 12 Other Functionals. *Theor. Chem. Acc.* **2008**, *120*, 215–241.
- (29) Krishnan, R.; Binkley, J. S.; Seeger, R.; Pople, J. A. Self-Consistent Molecular Orbital Methods. XX. A Basis Set for Correlated Wave Functions. *J. Chem. Phys.* **1980**, *72*, 650–655.
- (30) Vega-Rodriguez, A.; Alvarez-Idaboy, J. R. Quantum Chemistry and TST Study of the Mechanisms and Branching Ratios for the Reactions of OH with Unsaturated Aldehydes. *Phys. Chem. Chem. Phys.* **2009**, *11*, 7649–7658.
- (31) Galano, A. Mechanism and Kinetics of the Hydroxyl and Hydroperoxyl Radical Scavenging Activity of N-Acetylcysteine Amide. *Theor. Chem. Acc.* **2011**, *130*, 51–60.
- (32) Zhao, Y.; Truhlar, D. G. Density Functionals with Broad Applicability in Chemistry. *Acc. Chem. Res.* **2008**, *41*, 157–167.
- (33) Gonzales, C.; Schlegel, H. B. An Improved Algorithm for Reaction Path Following. *J. Chem. Phys.* **1989**, *90*, 2154–2162.
- (34) Gonzales, C.; Schlegel, H. B. Improved Algorithms for Reaction Path Following: Higher-Order Implicit Algorithms. *J. Phys. Chem.* **1991**, *95*, 5853–5860.
- (35) Lee, T. J.; Taylor, P. R. A Diagnostic for Determining the Quality of Single-Reference Electron Correlation Methods. *Int. J. Quantum Chem., Symp.* **1989**, *23*, 199–207.
- (36) Rienstra-Kiracofe, J. C.; Allen, W. D.; Schaefer, H. F., III. The $C_2H_5 + O_2$ Reaction Mechanism: High-Level ab Initio Characterizations. *J. Phys. Chem. A* **2000**, *104*, 9823–9840.
- (37) Schlegel, H. B.; Sosa, C. Ab Initio Molecular Orbital Calculations on $F+H_2 \rightarrow HF+H$ and $OH+H_2 \rightarrow H_2O+H$ using Unrestricted Møller-Plesset Perturbation Theory with Spin Projection. *Chem. Phys. Lett.* **1988**, *145*, 329–333.
- (38) Ignatyev, I. S.; Xie, Y.; Allen, W. D.; Schaefer, H. F. Mechanism of the $C_2H_5 + O_2$ Reaction. *J. Chem. Phys.* **1997**, *107*, 141–155.
- (39) Montgomery, J. A.; Frisch, M. J., Jr.; Ochterski, J. W.; Petersson, G. A. A Complete Basis Set Model Chemistry. VI. Use of Density Functional Geometries and Frequencies. *J. Chem. Phys.* **1999**, *110*, 2822–2827.
- (40) Alecu, I. M.; Truhlar, D. G. Computational Study of the Reactions of Methanol with the Hydroperoxyl and Methyl Radicals. 1. Accurate Thermochemistry and Barrier Heights. *J. Phys. Chem. A* **2011**, *115*, 2811–2829.
- (41) Nicolaides, A.; Rauk, A.; Glukhovtsev, M. N.; Radom, L. Heats of Formation from G2, G2(MP2), and G2(MP2,SVP) Total Energies. *J. Phys. Chem.* **1996**, *100*, 17460–17464.
- (42) Lias, S. G.; Bartmess, J. E.; Liebman, J. F.; Holmes, J. L.; Levin, R. D.; Mallard, W. G. Atomic Heats of Formation at 298K and 0K. *Gas-Phase Ion and Neutral Thermochemistry*; Journal of Physical and Chemical Reference Data, Vol. 17, Suppl. 1; American Chemical Society and American Institute of Physics: Washington, DC, and New York, 1988.
- (43) Frisch, M. J.; Trucks, G. W.; Schlegel, H. B.; Scuseria, G. E.; Robb, M. A.; Cheeseman, J. R.; Scalmani, G.; Barone, V.; Mennucci, B.; Petersson, G. A.; et al. *Gaussian 09*, revision B.01; Gaussian, Inc.: Pittsburgh, PA, 2009.
- (44) Cavalli, F.; Barnes, I.; Becker, K. H.; Wallington, T. J. Atmospheric Oxidation Mechanism of Methyl Propionate. *J. Phys. Chem. A* **2000**, *104*, 11310–11317.
- (45) Duncan, W. T.; Bell, R. L.; Truong, T. N. TheRate: Program for ab Initio Direct Dynamics Calculations of Thermal and Vibrational State Selected Rate Constants. *J. Comput. Chem.* **1998**, *19*, 1039–1052.
- (46) Ayala, P. Y.; Schlegel, H. B. Identification and Treatment of Internal Rotation in Normal Mode Vibrational Analysis. *J. Chem. Phys.* **1998**, *108*, 2314–2326.
- (47) Eckart, C. The Penetration of a Potential Barrier by Electrons. *Phys. Rev.* **1930**, *35*, 1303–1309.
- (48) Jorgensen, S.; Gross, A. Theoretical Investigation of the Reaction between Carbonyl Oxides and Ammonia. *J. Phys. Chem. A* **2009**, *113*, 10284–10290.
- (49) Mandal, D.; Bagchi, S.; Das, A. K. Mechanism and Kinetics for the Reaction of O(3P) with DMSO: A Theoretical Study. *Chem. Phys. Lett.* **2012**, *551*, 31–37.
- (50) Andersen, V. F.; Ørnsø, K. B.; Jørgensen, S.; Nielsen, O. J.; Johnson, M. S. Atmospheric Chemistry of Ethyl Propionate. *J. Phys. Chem. A* **2009**, *113*, 5164–5179.
- (51) Ruscic, B.; Pinzon, R. E.; Morton, M. L.; Srinivasan, N. K.; Su, M.; Sutherland, J. W.; Michael, J. V. Active Thermochemical Tables: Accurate Enthalpy of Formation of Hydroperoxyl Radical, HO₂. *J. Phys. Chem. A* **2006**, *110*, 6592–6601.
- (52) Cox, J. D.; et al. *CODATA Key Values for Thermodynamics*; Hemisphere: New York, 1989.
- (53) Chase, M. W. Jr. *NIST-JANAF Thermochemical Tables*, 4th ed.; Journal of Physical and Chemical Reference Data, Monograph 9; American Chemical Society and American Institute of Physics: Washington, DC, and Woodbury, NY; 1998; pp 1–1951.
- (54) Steele, W. V.; Chirico, R. D.; Cowell, A. B.; Knipmeyer, S. E.; Nguyen, A. Thermodynamic Properties and Ideal-Gas Enthalpies of Formation for 2-Aminoisobutyric Acid (2-Methylalanine), Acetic Acid, (4-Methyl-3-penten-2-one), 4-Methylpent-1-ene, 2,2'-Bis(phenylthio)-propane, and Glycidyl Phenyl Ether (1,2-Epoxy-3-phenoxypropane). *J. Chem. Eng. Data* **1997**, *42*, 1052–1066.
- (55) Vilcu, R.; Perisanu, S. The Ideal Gas State Enthalpies of Formation of Some Monomers. *Rev. Roum. Chim.* **1980**, *25*, 619–624.
- (56) Tsang, W. Heats of Formation of Organic Free Radicals by Kinetic Methods. In *Energetics of Organic Free Radicals*; Martinho, S. J. A., Greenberg, A., Lieberman, J. F., Eds.; Blackie Academic and Professional: London, 1996; pp 22–58.